Two approaches for the analysis of masonry structures: micro and macro-modeling

Paulo B. Lourenço
Delft University of Technology, Faculty of Civil Engineering, P.O. Box 5048, 2600 GA Delft, the Netherlands, also at TNO Building and Construction Research
Presently back at the School of Engineering, University of Minho, Guimarães, Portugal

Jan G. Rots
Delft University of Technology, Faculty of Civil Engineering, P.O. Box 5048, 2600 GA Delft, the Netherlands, also at TNO Building and Construction Research

Johan Blaauwendraad
Delft University of Technology, Faculty of Civil Engineering, P.O. Box 5048, 2600 GA Delft, the Netherlands

Two models for the micro- and macro-analysis of masonry structures are presented. For the micro-modeling of masonry, an interface failure criterion that includes a straight tension cut-off, the Coulomb friction law and an elliptical cap is proposed. The inelastic behavior includes tensile strength softening, cohesion softening, compressive strength hardening/softening and coupling between tensile and shear failure. It is shown that the model is capable of describing the local interaction of both masonry components and of reproducing, in a detailed manner, observed experimental behavior. For the macro-modeling, an anisotropic continuum model that includes a Rankine type yield surface for tension and a Hill type yield surface for compression is proposed. Anisotropic elasticity is combined with anisotropic plasticity, in such a way that totally different behavior can be predicted along the material axes, both in tension and compression. It is shown that, for sufficiently large structures, the global response of masonry can be well predicted even without the inclusion of the local interaction between the masonry components.

Keywords: **Plasticity, composite yield criteria, softening, finite element analysis, masonry modeling.**

1 Introduction

Masonry is the oldest building material that still finds wide use in today's building industries. Important new developments in masonry materials and applications occurred in the last decades but the techniques to assemble bricks and blocks are essentially the same as the ones developed ten thousand years ago. Naturally, innumerable variations of masonry materials, techniques and

HERON, Vol. 40, No. 4 (1995) ISSN 0046-7316

applications occurred during the course of times, influenced by the local culture and wealth, the knowledge of materials and tools, the availability of material and architectural reasons.
The most important characteristic of masonry construction is its simplicity. Laying pieces of stone or bricks on top of each other, either with or without cohesion via mortar, is a simple, though adequate technique that has been successful ever since remote ages. Other important characteristics are the aesthetics, solidity, durability and low maintenance, versatility, sound absorption and fire protection. Loadbearing walls, infill panels to resist seismic and wind loads, prestressed masonry cores and low-rise buildings are examples of constructions where the use of structural masonry is presently competitive. However, innovative applications of structural masonry are hindered by the fact that the development of design rules has not kept pace with the developments for concrete and steel. The underlying reason is the lack of insight and models for the complex behavior of units, mortar, joints and masonry as a composite material. Existing calculation methods are mainly of empirical and traditional nature and the use of numerical tools for the analysis or design of masonry structures is rather incipient.
The fundamental point of today's research in structural masonry is thus to *rationalize the engineering design of structural masonry*. Considerable research effort has been made in the last two decades but progress has been hindered by the lack of communication between analysts and experimentalists. In fact, a combined experimental/numerical basis is the key to validate, extend and improve existing methods as indicated by the integrated research program of CUR (1994). At the present stage of knowledge, numerical simulations are fundamental to provide insight into the structural behavior and support the derivation of rational design rules but nonlinear finite element analyses will be always helpful for the *validation of the design of complex masonry structures under complex loading conditions*. In particular, computations beyond the limit load down to a possibly lower residual load are needed to assess the safety of the structure. Aside from failure analysis, also the serviceability limit states can be successfully validated with numerical analyses. Another important aspect is the safety of existing structures under existing or new loading conditions, with an emphasis in the preservation of historical structures. Reliable numerical models are necessary to *assess and strengthen existing masonry structures*. The final point is the need to *improve the performance of masonry buildings in underdeveloped countries*. It is remarkable that over one-third of the world's population still leaves in earth houses today, Dethier (1982), for modern western technology has failed, both financially and socially, to satisfy the local increasing demand of cheap housing. Research must be carried on techniques that use local materials, are kept as simple as possible and do not increase significantly the cost, which is not merely a question of transferring existing technology.
At the present stage, we have introduced the importance of sophisticated numerical tools, capable of predicting the behavior of the structure from the linear stage, through cracking and degradation until complete loss of strength. This objective can only be achieved if accurate and robust constitutive models are complemented with advanced solution procedures of the system of equations which results from the finite element discretization (it is tacitly assumed that the finite element method is adopted to simulate the structural behavior). The present article focuses on the nonlinear analysis of unreinforced masonry structures which can be approximated as being in a state of plane stress, such as panels and shear walls. The structures under consideration are subjected to short time static loads, which are not necessarily proportional but, in essence, monotonical. The main goal of this article is to present advanced numerical tools for the analysis of masonry structures.

The proposed models were developed in the doctoral thesis project of the first author and have been implemented in the DIANA finite element code, which has been used in all the analyses.

2 Approaches towards computational modeling of masonry structures

Only recently the masonry research community began to show interest in sophisticated numerical tools as an opposition to the prevailing tradition of rules-of-thumb and empirical formulae. The fact that little importance has been attached to numerical aspects is confirmed by the absence of any well established models. The difficulties in adopting existing numerical tools from more advanced research fields, namely the mechanics of concrete, rock and composite materials, are hindered by the particular characteristics of masonry. Masonry is a composite material that consists of units and mortar joints, see Fig. 1a. A comprehensive analysis of masonry, hereby denoted detailed *micro-modeling*, must then include a representation of units, mortar and the unit/mortar interface, see Fig. 1b. In this case units and mortar in the joints are represented by continuum elements whereas the unit-mortar interface is represented by discontinuous elements. The Young's modulus, Poisson's ratio and, optionally, inelastic properties of both unit and mortar are taken into account. The interface represents a potential crack/slip plane with initial dummy stiffness to avoid inter-penetration of the continuum. This enables the combined action of unit, mortar and interface to be studied under a magnifying glass. Such a representation of masonry leads to large memory and time requirements and a simplified micro-modeling of masonry will be preferably used here, see Fig. 1c. In this case expanded units are represented by continuum elements whereas the behavior of the mortar joints and unit-mortar interface is lumped in discontinuous elements. Each joint, consisting of mortar and the two unit-mortar interfaces, is lumped into an "average" interface

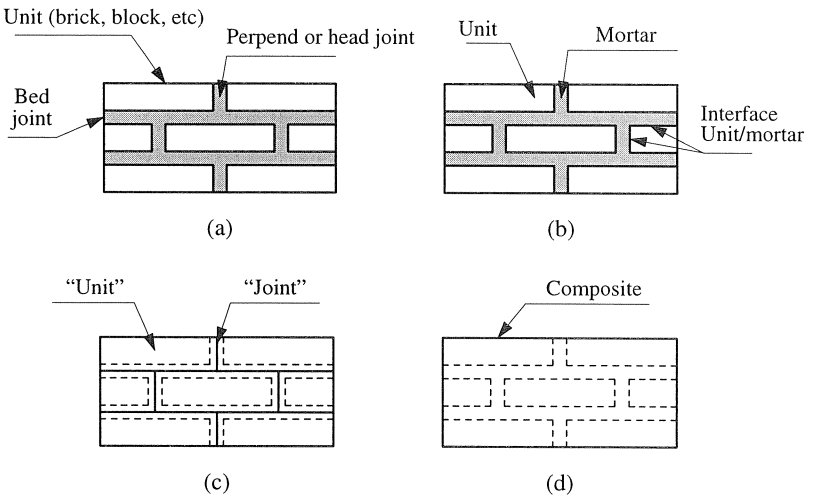

Fig. 1. Modeling strategies for masonry structures: (a) masonry sample; (b) detailed micro-modeling; (c) simplified micro-modeling; (d) macro-modeling.

while the units are expanded in order to keep the geometry unchanged. Masonry is thus considered as a set of elastic blocks bonded by potential fracture/slip lines at the joints. Accuracy is lost since Poisson's effect of the mortar is not included.

Micro-modeling approaches are suited for small structural elements with particular interest in strongly heterogeneous states of stress and strain. The primary aim of micro-modeling is to closely represent masonry from the knowledge of the properties of each constituent and the interface. The necessary experimental data must be obtained from laboratory tests in the constituents and small masonry samples. Several attempts to use interfaces for the modeling of masonry were carried out in the last decade with reasonably simple models, see e.g. Anthoine (1992) for references. In particular, gradual softening behavior and all failure mechanisms, namely tensile, shear and compressive failure, have not been fully included.

In large and practice-oriented analyses the knowledge of the interaction between units and mortar is, generally, negligible for the global structural behavior. In these cases a different approach can be used, hereby denoted *macro-modeling*, where a distinction between individual units and joints is not made, see Fig. 1d. Instead the material is regarded as an anisotropic composite and a relation is established between average masonry strains and average masonry stresses. This is clearly a phenomenological approach, meaning that the material parameters must be obtained from masonry tests of sufficient size under homogeneous states of stress. A complete macro-model must reproduce an orthotropic material with different tensile and compressive strengths along the material axes as well as different inelastic behavior for each material axis.

A reduced number of orthotropic material models specific for masonry has been proposed, see e.g. Anthoine (1992) and Lourenço (1996) for references. It is not surprising that so few macro-models have been implemented due to the intrinsic complexity of introducing orthotropic behavior. The models proposed in the past have not been widely accepted due to the difficulties of formulating robust numerical algorithms and representing satisfactorily the inelastic behavior.

It is noted that one modeling strategy cannot be promoted over the other because different application fields exist for micro- and macro-models. Micro-modeling studies are necessary to give a better understanding about the local behavior of masonry structures. This type of modeling applies notably to structural details, but also to modern building systems like those of concrete or calcium-silicate blocks, where window and door openings often result in piers that are only a few block units in length. These piers are likely to determine the behavior of the entire wall and individual modeling of the blocks and joints is then to be preferred. Macro-models are applicable when the structure is composed of solid walls with sufficiently large dimensions so that the stresses across or along a macro-length will be essentially uniform. Clearly, macro-modeling is more practice oriented due to the reduced time and memory exigencies as well as a user-friendly mesh generation. This type of modeling is most valuable when a compromise between accuracy and efficiency is needed.

3 Basics of single and multisurface plasticity

In this study the finite element method is adopted to simulate the structural behavior. A mathematical description of the material behavior, which yields the relation between the stress and strain tensor in a material point of the body, is necessary for this purpose. This mathematical description is commonly named a constitutive model. Constitutive models will be developed here in a plasticity framework according to a phenomenological approach in which the observed mechanisms are represented in such a fashion that simulations are in reasonable agreement with experiments. It is not realistic to try to formulate constitutive models which fully incorporate all the interacting mechanisms of a specific material because any constitutive model or theory is a simplified representation of reality. It is believed that more insight can be gained by tracing the entire response of a structure than by modeling it with a highly sophisticated material model or theory which does not result in a converged solution close to the failure load. The theory of plasticity is well established and sound numerical algorithms have been implemented, e.g. Simo *et al.* (1988). It is a natural constitutive description for metals, but it can also be used for quasi-brittle cementitious materials loaded in triaxial compression and shear-compression problems where inelastic non-recoverable strains are observed. The incapability of the theory to reproduce the elastic stiffness degradation of quasi-brittle materials subjected mainly to tension cannot be accepted for cyclic loading but, for monotonic loading conditions, good results have been found, e.g. Feenstra (1993) and Lourenço (1996).

In the following, we introduce the basic aspects of the theory of single and multisurface rate independent plasticity. A fundamental notion in the plasticity theory is the existence of a yield function that bounds the elastic domain. Yielding can only occur if the stresses σ satisfy the general yield criterion

$$f(\sigma, \bar{\sigma}(\kappa)) = 0 \tag{1}$$

where the yield stress value $\bar{\sigma}$ is a function, commonly named hardening law, of the scalar κ, which is introduced as a measure for the amount of hardening or softening. In general, however, it is extremely complex to describe the material behavior with a unique yield surface in an appropriate manner and one must resort to the theory of multisurface plasticity. In this case the elastic domain is defined by a number of functions $f_i < 0$ which define a composite yield surface. Loading/unloading can be conveniently established in standard Kuhn-Tucker form by means of the conditions.

$$\dot{\lambda}_i \geq 0 \quad f_i \leq 0 \quad \dot{\lambda}_i f_i = 0 \tag{2}$$

where $\dot{\lambda}_i$ is the plastic multiplier rate. Plastic behavior is characterized by a non-unique stress-strain relationship with the presence of irreversible strains on load removal. This is obtained by the usual decomposition of the strain rate vector $\dot{\varepsilon}$ in an elastic, reversible part, $\dot{\varepsilon}^e$ and a plastic, irreversible part, $\dot{\varepsilon}^p$

$$\dot{\varepsilon} = \dot{\varepsilon}^e + \dot{\varepsilon}^p \tag{3}$$

where the elastic strain rate is related to the stress rate by the elastic (constitutive) stiffness matrix $\mathbf{D}$ as

$$\dot{\sigma} = \mathbf{D}\dot{\varepsilon}^{e} \tag{4}$$

For single surface plasticity, the assumption of an associated flow rule yields

$$\dot{\varepsilon}^{p} = \dot{\lambda}\frac{\partial f}{\partial \sigma} \tag{5}$$

and a non-associated flow rule yields

$$\dot{\varepsilon}^{p} = \dot{\lambda}\frac{\partial g}{\partial \sigma} \tag{6}$$

where g is the plastic potential. In the case of strain hardening (or softening) the scalar $\dot{\kappa}$ reads

$$\dot{\kappa} = \dot{\varepsilon}^{eps} \tag{7}$$

where the equivalent plastic strain rate $\dot{\varepsilon}^{eps}$ must be always positive and increasing. The simplest combination of this kind which is dimensionally correct is

$$\dot{\kappa} = \dot{\varepsilon}^{eps} = \sqrt{(\dot{\varepsilon}^{p})^{T}\dot{\varepsilon}^{p}} \tag{8}$$

Another possibility is to define the equivalent plastic strain rate from the plastic work per unit of volume in the form

$$\dot{W}^{p} = \bar{\sigma}\dot{\varepsilon}^{eps} = \sigma^{T}\dot{\varepsilon}^{p} \tag{9}$$

which gives

$$\dot{\kappa} = \dot{\varepsilon}^{eps} = \frac{1}{\bar{\sigma}}\sigma^{T}\dot{\varepsilon}^{p} \tag{10}$$

For multisurface plasticity the intersection of the different yield surfaces defines corners. Without lack of generality it is assumed that the composite yield surface is defined by two yield surfaces. According to Koiter's generalization, Koiter (1953), the plastic strain rate $\dot{\varepsilon}^{p}$ in the corner is obtained from a linear combination of the plastic strain rates of the two yield surfaces, reading

$$\dot{\varepsilon}^{p} = \dot{\varepsilon}_1^{p} + \dot{\varepsilon}_2^{p} = \dot{\lambda}_1\frac{\partial g^{1}}{\partial \sigma} + \dot{\lambda}_2\frac{\partial g^{2}}{\partial \sigma} \tag{11}$$

The yield surfaces can also be explicitly coupled by introducing composite hardening scalar rates $\dot{\kappa}_1^{c}$ and $\dot{\kappa}_2^{c}$

$$\dot{\kappa}_1^{c} = \dot{\kappa}_1^{c}(\dot{\kappa}_1, \dot{\kappa}_2) \qquad \dot{\kappa}_2^{c} = \dot{\kappa}_2^{c}(\dot{\kappa}_1, \dot{\kappa}_2) \tag{12}$$

where $\dot{\kappa}_1 = \dot{\kappa}_1(\dot{\varepsilon}_1^{p})$ and $\dot{\kappa}_2 = \dot{\kappa}_2(\dot{\varepsilon}_2^{p})$ are defined according to one of eqs. (8,10). The superscript c refers to composite.

4 Micro-modeling: A composite interface model for masonry

Micro-models are, probably, the best tool available to understand the behavior of masonry. The benefit of using such an approach is that all the different failure mechanisms can be considered. In the following, attention is given to a simplified modeling strategy, in which interface elements are used as potential crack, slip or crushing planes. A composite interface model, which includes a tension cut-off for mode I failure, a Coulomb friction envelope for mode II failure and a cap mode for compressive failure, is presented. In addition, interface elements are considered to model potential cracks in the units. The complete description of the numerical implementation in modern plasticity concepts is given elsewhere, see Lourenço (1996), and will not be reviewed here.

4.1 Adopted modeling strategy

An accurate micro-model must include all the basic types of failure mechanisms that characterize masonry, viz. (a) cracking of the joints, (b) sliding along the bed or head joints at low values of normal stress, (c) cracking of the units in direct tension, (d) diagonal tension cracking of the units at values of normal stress sufficient to develop friction in the joints and (e) "masonry crushing", commonly identified with splitting of units in tension as a result of mortar dilatancy at high values of normal stress, as illustrated in Fig. 2. It is clear from the described phenomena that (a,b) are joint mechanisms, (c) is a unit mechanism and (d,e) are combined mechanisms involving units and joints. The question remains of how to consider all phenomena in the model. The approach followed here is to concentrate all the damage in the relatively weak joints and in potential pure tension cracks in the units placed vertically in the middle of each unit, see Fig. 3. These potential cracks in the units are able to reproduce a jump from one head joint to the other (immediately below or above), which is a typical masonry characteristic. The joint interface yield criterion has then to include all the mechanisms referred above except uniaxial tensile cracking of the unit. By limiting the compressive/shear stress combinations, diagonal tension cracking of the units and masonry crushing, failure mechanisms (d,e) in Fig. 2, can be incorporated in the model.
Interface elements permit discontinuities in the displacement field and their behavior is described in terms of a relation between the tractions $\mathbf{t}$ and relative displacements $\Delta\mathbf{u}$ across the interface. The linear elastic relation between these generalized stresses and strains can be written in the standard form as

$$\sigma = \mathbf{D}\varepsilon \tag{13}$$

where, for a 2D configuration, $\sigma = \{\sigma, \tau\}^T$, $\mathbf{D} = diag\ \{k_n, k_s\}$ and $\varepsilon = \{\Delta u_n, \Delta u_s\}^T$, with n and s denoting the normal and shear components, respectively. The elastic stiffness matrix $\mathbf{D}$ can be obtained from the properties of the two masonry components (units and mortar) and the thickness of the joint. Fig. 3 showed that, due to the zero thickness inherent to the interface element formulation, the size of the units has to be expanded by the mortar thickness h_m in both directions. It follows that the elastic properties of the "expanded unit" and the "interface joint" must be adjusted to yield correct results. Due to the relative dimensions of mortar and unit, it is assumed that the elastic properties of the unit remain unchanged. Then the components of the elastic stiffness matrix $\mathbf{D}$ read, CUR (1994),

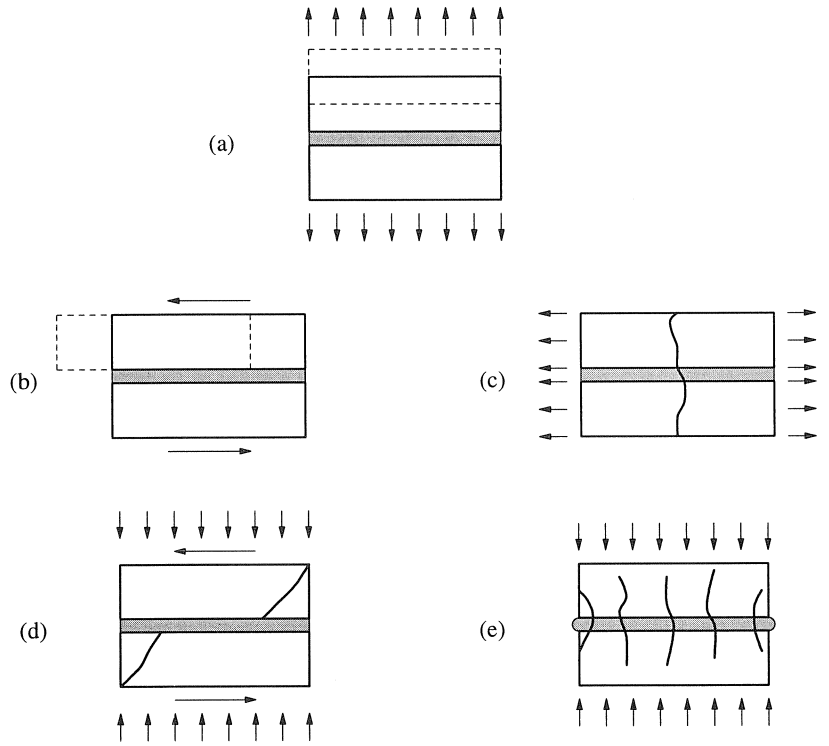

Fig. 2. Masonry failure mechanisms:
(a) joint tension cracking; (b) joint slipping; (c) unit direct tension cracking; (d) unit diagonal tension cracking; (e) masonry crushing.

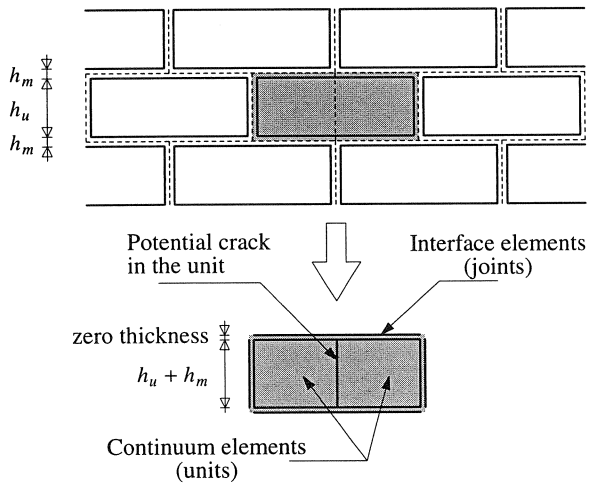

Fig. 3. Suggested modeling strategy. Units (u), which are expanded in both directions by the mortar thickness, are modeled with continuum elements. Mortar joints (m) and potential cracks in the units are modeled with zero-thickness interface elements.

$$k_n = \frac{E_u E_m}{h_m(E_u - E_m)} \qquad k_s = \frac{G_u G_m}{h_m(G_u - G_m)} \tag{14}$$

where E_u and E_m are the Young's moduli, G_u and G_m are the shear moduli, respectively, for unit and mortar and h_m is the actual thickness of the joint. The stiffness values obtained from these formulae do not correspond to a penalty approach, which means that overlap of neighboring units subjected to compression will become visible. This is a phenomenological representation of masonry crushing because the failure process in compression is, in reality, explained by the microstructure of units and mortar and the interaction between them.

4.2 *The composite interface model*

Cap models originated in the field of soil mechanics. The introduction of a spherical cap for the Drucker-Prager model was firstly made by Drucker *et al.* (1957) for the purpose of describing plastic compaction and enhance the behavior in hydrostatic compression. Since then the name "cap model" has been adopted for a broad set of models which include a compressive cap, e.g the well-known Cam-clay model of Roscoe and Burland (1968). Recently the numerical algorithm has been revised by Hofstetter *et al.* (1993) with the use of unconditionally stable closest point projection return mappings, tangent operators consistent with the integration algorithm and proper handling of the corners. Cap models have been, in general, limited to associated plasticity and hardening of the cap while the other yield surfaces remained in ideal plasticity.

For the application envisaged here the behavior found experimentally leads to a more complex model. Masonry joints have extremely low dilatancy and the model must be formulated in the context of non-associated plasticity. Also softening behavior should be included for all modes of the composite yield surface.

The rate independent interface model is defined by a convex composite yield criterion which consists of a tension cut-off $f_1(\sigma, \kappa_1)$, the Coulomb friction model $f_2(\sigma, \kappa_2)$, and an elliptical cap $f_3(\sigma, \kappa_3)$, see Fig. 4.

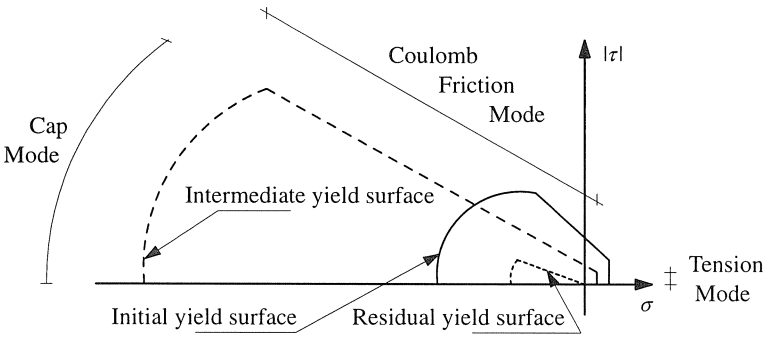

Fig. 4. Proposed model for interfaces. An "interface cap model".

4.2.1 The tension cut-off criterion

For the tension cut-off, the yield function reads

$$f_1(\sigma, \kappa_1) = \sigma - \bar{\sigma}_1(\kappa_1) \tag{15}$$

where the yield value $\bar{\sigma}_1$ reads (exponential softening)

$$\bar{\sigma}_1 = f_t \exp\left(-\frac{f_t}{G_f^I}\kappa_1\right) \tag{16}$$

In the above f_t is the tensile strength of the joint or, more precisely, of the unit-mortar interface, which is, generally, the weakest link, and G_f^I is the mode I fracture energy. An associated flow rule and a strain softening hypothesis are considered. Assuming that only the normal plastic relative displacement controls the softening behavior, eq. (7) yields

$$\dot{\kappa}_1 = |\Delta \dot{u}_n^p| = \dot{\lambda}_1 \tag{17}$$

4.2.2 The Coulomb friction criterion

For the Coulomb friction mode, the yield function reads

$$f_2(\sigma, \kappa_2) = |\tau| + \sigma \tan\phi(\kappa_2) - \bar{\sigma}_2(\kappa_2) \tag{18}$$

where the yield value $\bar{\sigma}_2$ reads (exponential softening)

$$\bar{\sigma}_2 = c \exp\left(-\frac{c}{G_f^{II}}\kappa_2\right) \tag{19}$$

In the above c is the cohesion of the unit-mortar interface, ϕ is the friction angle and G_f^{II} is the mode II fracture energy. A non-associated plastic potential g_2,

$$g_2 = |\tau| + \sigma \tan\psi - c \tag{20}$$

with a dilatancy angle ψ and a strain softening hypothesis are considered. Assuming that the softening behavior is controlled by the shear plastic relative displacement, eq. (7) yields

$$\dot{\kappa}_2 = |\Delta \dot{u}_s^p| = \dot{\lambda}_2 \tag{21}$$

4.2.3 The compressive cap criterion

For the cap mode, a centered ellipsoid is used. The yield function is now given by

$$f_3(\sigma, \kappa_3) = \sigma^2 + C_{ss}\tau^2 - (\bar{\sigma}_3(\kappa_3))^2 \tag{22}$$

where C_{ss} is a material parameter which controls the contribution of the shear stress to failure and $\bar{\sigma}_3$ is the yield value.

For the hardening/softening behavior the law shown in Fig. 5 is adopted, where the subscripts *i*, *m*, *p* and *r* of the yield value $\bar{\sigma}$ denote respectively, the initial, medium, peak and residual values. The peak value $\bar{\sigma}_p$ equals the masonry compressive strength f_m. This approach, in which several κ and $\bar{\sigma}$ values are adjusted to fit the stress-displacement curve obtained experimentally, can be used for interface elements because a direct relation between stresses and displacements is established. Using matrix notation, eq. (22) can be rewritten in a form more amenable to computational implementation, as

$$f_3(\sigma, \kappa_3) = \tfrac{1}{2}\sigma^T \mathbf{P}\sigma - -(\bar{\sigma}_3(\kappa_3))^2 \tag{23}$$

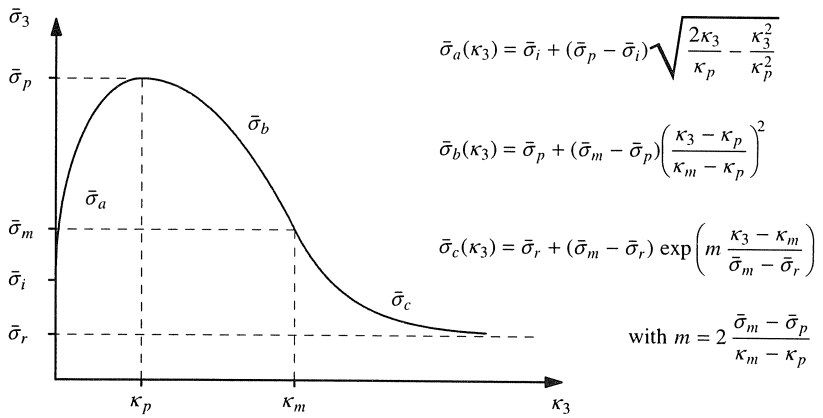

Fig. 5. Hardening/softening law for cap mode.

where the projection matrix **P** equals *diag* {2,2 C_{ss}}. An associated flow rule and a strain hardening/softening hypothesis are considered. This yields, upon substitution in eq. (8),

$$\dot{\kappa}_3 = \dot{\lambda}_3\sqrt{(\mathbf{P}\sigma)^T(\mathbf{P}\sigma)} \tag{24}$$

4.2.4 Corner regimes

The corners of the composite yield surface are singular points that have been handled according to Lourenco (1996).

One important feature of the composite yield surface is the coupling of tension and shear softening because both phenomena are related to the bond or adhesion between unit and mortar. Here, isotropic softening is assumed, which means that the percentages of the cohesion and tensile strength softening are equal throughout the entire degradation process. Experimental results for mixed (shear-tension) stress paths are not available because, as reported by Van der Pluijm (1993),

even for low compressive confining stresses brittle results are found with potential instability of the test set-up. The assumption of isotropic softening comes only by physical reasoning because any amount of coupling between tension and shear can be introduced in the model. However, it seems natural to assume equal degradation of strength because both phenomena are due to the breakage of the same bridges that exist at micro-level between unit and mortar.

The cap and shear modes are assumed to be uncoupled. Again, the physical reasoning behind this assumption is clear. The shear mode represents a unit-mortar interface phenomenon whereas the cap mode represents, basically, masonry crushing.

4.3 *Example of application*

Traditionally, experiments in shear walls have been adopted by the masonry community as the most common in-plane large test. Yet, little understanding still exists about the behavior of this type of structures. In this article, attention is devoted to shear wall tests carried out in the Netherlands, see Raijmakers and Vermeltfoort (1992) and CUR (1994), because most of the parameters necessary to characterize the material model are available from micro-experiments.

The analyzed shear wall, here denoted by wall JD, has a width/height ratio of one with dimensions $990 \times 1000\ mm^2$, built up with 18 courses, from which 16 courses are active and 2 courses are clamped in steel beams, see Fig. 6. In this figure, the arrow with a circle indicates a displacement. The wall is made of wire-cut solid clay bricks with dimensions $210 \times 52 \times 100\ mm^3$ and 10 mm thick mortar, prepared with a volumetric cement:lime:sand ratio of 1:2:9. A vertical precompression uniformly distributed force equal to $0.30\ N/mm^2$ is applied, before a horizontal load is monotonically increased under top displacement control d in a confined way, i.e. keeping the bottom and top boundaries horizontal and precluding any vertical movement, see Fig. 6.

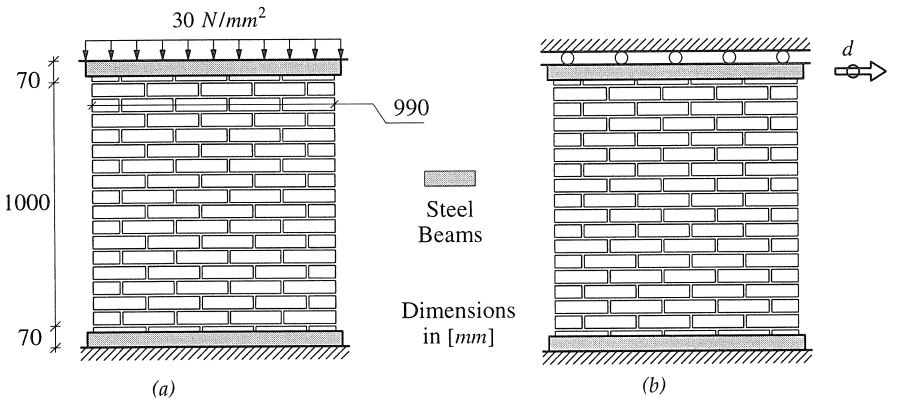

Fig. 6. Loads for wall JD: (a) phase 1 – vertical loading; (b) phase 2 – horizontal loading under displacement control.

The experimental crack patterns for two successfully carried out tests are shown in Fig. 7. Horizontal tension cracks develop at the bottom and top of the wall at an early loading stage but, ultimately, a diagonal stepped crack leads to collapse, simultaneously with cracks in the bricks and crushing of the compressed toes.

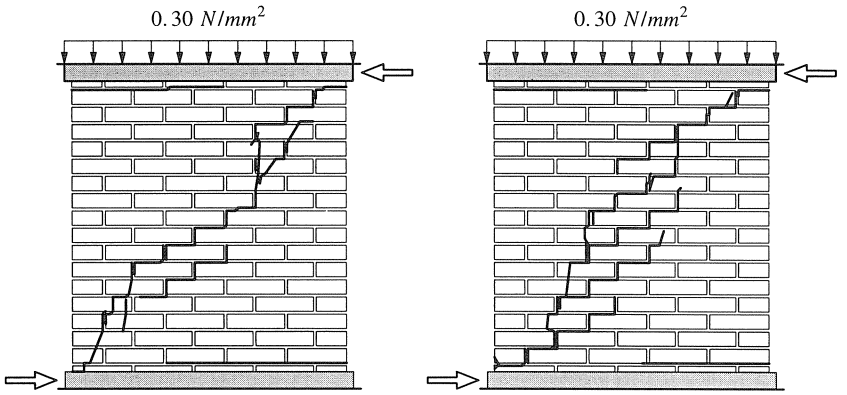

Fig. 7. Wall JD. Experimental failure patterns for two different tests.

For the numerical analysis, units are represented by plane stress continuum elements (8-noded) while line interface elements (6-noded) are adopted for the joints and for the potential vertical cracks in the middle of the unit. Each unit is modeled with 4×2 elements. For the joints, the composite interface model described in this article is adopted and, for the potential cracks in the units, a simple mode I cracking model with exponential tensile softening and immediate drop to zero of the shear stress after initiation of the crack is assumed. The analysis was carried out with direct displacement control.

The micro-properties for the different materials are obtained from Raijmakers and Vermeltfoort (1992) and CUR (1994), see Table 1 to Table 3. Note that an elastic dummy stiffness is considered for the potential cracks in the bricks. The hardening/softening law for the cap mode is defined by the set $\{\bar{\sigma}_3, \kappa_3\}_i = \{(f_m/3, 0.0);(f_m, 0.09);(f_m/2, 0.49);(f_m/7, +\infty)\}$

Table 1. Wall JD. Properties for the potential brick cracks.

k_n	k_s	f_t	G_f^I
1.0×10^6 N/mm^3	1.0×10^6 N/mm^3	2.0 N/mm^2	0.08 N/mm^2

Table 2. Wall JD. Elastic properties for the bricks and joints.

Brick		Joint	
E	v	k_n	k_s
16700 N/mm^2	0.15	82;110;82 N/mm^3	36;50;36 N/mm^3

Table 3. Wall JD. Inelastic properties for the joints.

Tension		Shear				Cap	
f_t	G_f^I	c	$\tan\phi$	$\tan\psi$	G_f^{II}	f_m	C_{ss}
0.25 N/mm^2	0.018 Nmm/mm^2	1.4 f_t N/mm^2	0.75	0.0	0.125 Nmm/mm^2	10.5 N/mm^2	9.0

The comparison between numerical and experimental load-displacement diagrams is shown in Fig. 8. The experimental behavior is satisfactorily reproduced and the collapse load can be well estimated. The sudden load drops are due to cracking in a single integration point of the potential cracks in a brick and opening of each complete crack across one brick. The walls behave in a rather ductile manner, which seems to confirm the idea that confined masonry can withstand substantial post-peak deformation with reduced loss of strength.

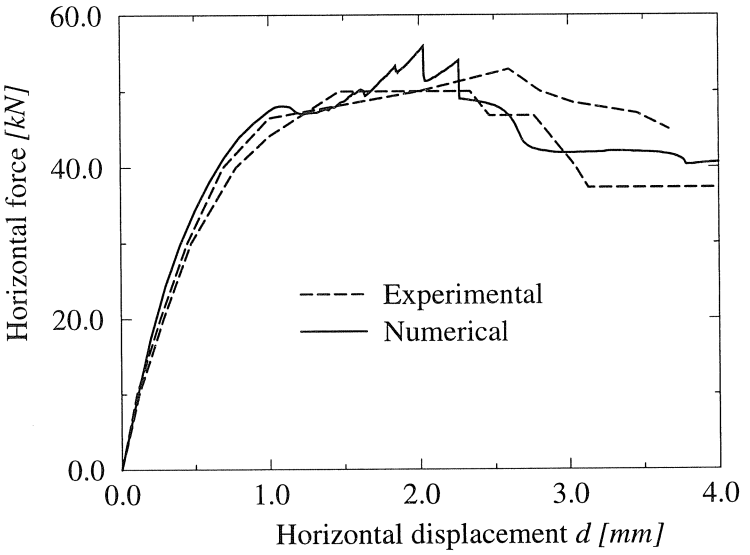

Fig. 8. Wall JD. Load – displacement diagrams.

The behavior of the wall is well captured by the model as illustrated in Fig. 9 and Fig. 10. In these figures, the word "damage" is used for the equivalent plastic strain from each mode of the composite interface model. Note that the "damage" of the compressive cap is only shown in the softening regime, not during hardening. Initially, two horizontal tension cracks develop at the bottom and top of the wall. A stepped diagonal crack through head and bed joints immediately follows. This crack starts in the middle of the wall and is accompanied by initiation of cracks in the bricks, see Fig. 9. Under increasing deformation, the crack progresses in the direction of the supports and,

finally, a collapse mechanism is formed with crushing of the compressed toes and a complete diagonal crack through joints and bricks, see Fig. 10.

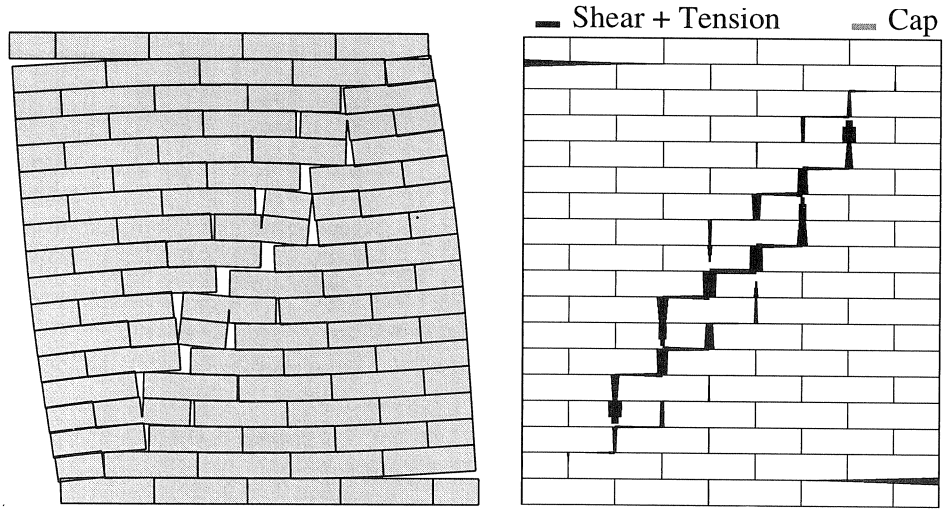

Fig. 9. Wall JD. Results of the analysis at a displacement of 2.0 mm: (a) deformed mesh; (b) damage.

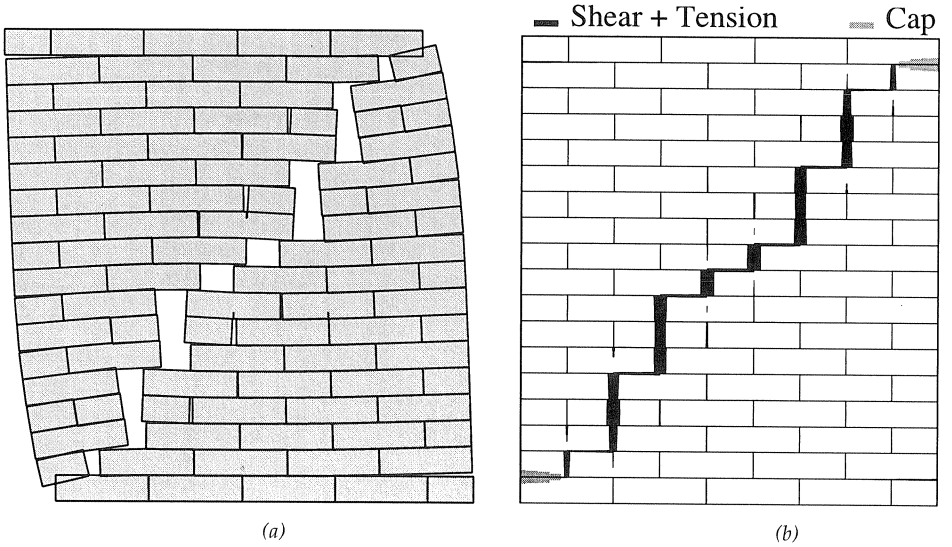

Fig. 10. Wall JD. Results of the analysis at a displacement of 4.0 mm: (a) deformed mesh; (b) damage.

5 Macro-modeling: An anisotropic continuum model

The analysis of masonry structures built from a large number of units and joints can only be carried out with macro-models, in which a relation between average stresses and strains in the composite material is established. The effective constitutive behavior of masonry features anisotropy arising from the geometrical arrangement of units and mortar, even if the properties of these constituents are isotropic. It might be expected that, to model masonry as a composite, sound numerical implementations of anisotropic plasticity models, which are generalizations of existing isotropic realizations, will be required.

The modern plasticity framework is general enough to apply equally well to both isotropic and anisotropic plasticity models. However, it appears that while many anisotropic plasticity models have been proposed from purely theoretical and experimental standpoints, e.g. Hill (1948) and Tsai and Wu (1971), only a few numerical implementations and calculations have actually been carried out. An example is given by the work of de Borst and Feenstra (1990) which fully treated the implementation of an elastic-perfectly-plastic Hill yield criterion. In principle, hardening behavior could be simulated with the fraction model of Besseling (1958) but not much effort has been done in this direction. A more recent attempt is given for example in Swan and Cakmak (1994), which included linear tensorial hardening in the Hill yield criterion.

This article presents a composite yield criterion suitable for the modeling of anisotropic materials under plane stress conditions. Individual yield criteria are considered for tension and compression, according to different failure mechanisms. The former is associated with a localized fracture process, denoted by cracking of the material, and, the latter, is associated with a more distributed fracture process which is usually termed as crushing of the material.

5.1 *The anisotropic continuum model*

An accurate analysis of masonry structures in a macro-modeling (or composite) perspective requires a material description for all stress states. The yield surface to be presented next combines the advantages of modern plasticity concepts with a powerful representation of anisotropic material behavior, which includes different hardening/softening behavior along each material axis.

It is noted that a representation of an orthotropic yield surface in terms of principal stresses only is not possible. For plane stress situations, which is the case of the present study, a graphical representation in terms of the full stress vector (σ_x, σ_y, τ_{xy}) is necessary. The material axes are assumed to be defined by the bed joints direction (x direction) and the head joints direction (y direction). Other possible representation can be obtained in terms of principal stresses and an angle θ. The angle θ measures the rotation between the principal stress axes and the material axes. Clearly, different principal stress diagrams are found according to different values of θ.

The approach followed here consists of an extension of conventional formulations for isotropic quasi-brittle materials to describe orthotropic behavior. Formulations of isotropic quasi-brittle materials behavior consider, generally, different inelastic criteria for tension and compression.

In the present article, an extension of the work of Feenstra and de Borst (1996), who utilized this approach for concrete with a Rankine and a Drucker-Prager criterion, will be presented. In order to

model orthotropic material behavior, a Hill type* yield criterion for compression and a Rankine type** yield criterion for tension, see Fig.11, will be proposed. Coupling between the two yield criteria is not present. The complete description of the numerical implementation has been presented elsewhere, see Lourenco (1996), and will not be reviewed here.

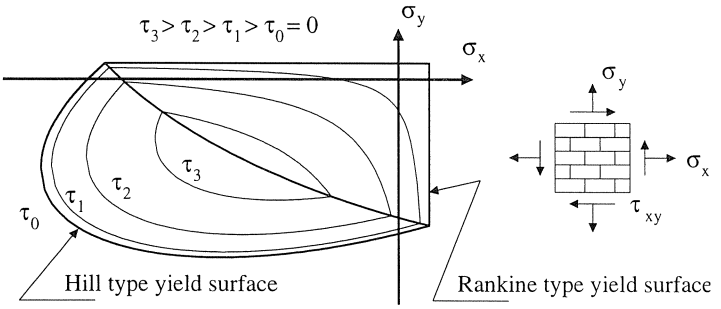

Fig. 11. Proposed composite yield surface with iso-shear stress lines. Different strength values for tension and compression along each material axis.

5.1.1 Discretization aspects

The softening behavior of masonry is modeled with a smeared approach in which the damaged material is still considered as a continuum in which the notions of stress and strain apply. With this assumption, the localized damage can be represented by the scalar κ, which is related by an equivalent length to the released energy per unit cracked area, G_f. In a finite element calculation this equivalent length should correspond to a representative dimension of the mesh size so that the results obtained are objective with regard to mesh refinement, see Bažant and Oh (1983).
The equivalent length, denoted by h, depends in general on the chosen element type, element size, element shape, integration scheme and even on the particular problem considered. In this study it is assumed that the equivalent length is related to the area of an element by, see Feenstra (1993),

$$h = \alpha_h \sqrt{A_e} = \alpha_h \left(\sum_{\zeta=1}^{n_\zeta} \sum_{\eta=1}^{n_\eta} \det(\mathbf{J}) w_\zeta w_\eta \right)^{1/2} \tag{25}$$

in which w_ζ and w_η are the weight factors of the Gaussian integration rule as it is tacitly assumed that the elements are always integrated numerically. The local, isoparametric coordinates of the integration points are given by ζ and η. The factor α_h is a modification factor which is equal to one for quadratic elements and equal to $\sqrt{2}$ for linear elements, see Rots (1988).

---

* The word *type* is used here because the original author, see Hill (1948), assumed a three-dimensional formulation. The influence of the out-of-plane direction is generally unknown and will not be considered. The adopted yield surface should, in fact, be considered as a particular case of the complete quadratic formulation from Tsai and Wu (1971).

** The word *type* is used here because the Rankine yield criterion represents the material strength along the maximum principal stress. For an anisotropic material such definition is clearly not possible. The proposed yield surface for tension will be derived from the original Rankine yield criterion but represents solely a fit of experimental results.

The inelastic work g_f is defined by the integral

$$g_f = \int \sigma^T d\varepsilon = \int \sigma^T d\varepsilon^p \tag{26}$$

which corresponds to the area under the stress-strain diagram for uniaxial loading.
Assuming that the inelastic work g_f is uniformly distributed over the equivalent length, the relation between the fracture energy G_f and the work g_f is given by

$$g_f = \frac{G_f}{h} \tag{27}$$

This results in a material model related to the energy which has to be dissipated due to the irreversible damage in the material. The concept of an equivalent length has been used extensively in the analysis of concrete structures. In this study, this concept will be used to model the tensile and compressive softening behavior of masonry, although it is recognized that the latter mechanism is physically more a volume-driven process than a surface-driven process.

5.1.2 A Rankine type criterion

The expression for the Rankine yield criterion can be written, see Lourenco (1996), as

$$f_1 = \frac{(\sigma_x - \bar{\sigma}_t(\kappa_t)) + (\sigma_y - \bar{\sigma}_t(\kappa_t))}{2} + \sqrt{\left(\frac{(\sigma_x - \bar{\sigma}_t(\kappa_t)) + (\sigma_y - \bar{\sigma}_t(\kappa_t))}{2}\right)^2 + \tau_{xy}^2} \tag{28}$$

where the single scalar κ_t is used to control the amount of softening. Setting forth a Rankine type yield surface for an orthotropic material, with different tensile strengths along the x, y directions is now straightforward if eq. (28) is modified to

$$f_1 = \frac{(\sigma_x - \bar{\sigma}_{t1}(\kappa_t)) + (\sigma_y - \bar{\sigma}_{t2}(\kappa_t))}{2} + \sqrt{\left(\frac{(\sigma_x - \bar{\sigma}_{t1}(\kappa_t)) + (\sigma_y - \bar{\sigma}_{t2}(\kappa_t))}{2}\right)^2 + \alpha\tau_{xy}^2} \tag{29}$$

where the parameter α, which controls the shear stress contribution to failure, reads

$$\alpha = \frac{f_{tx} f_{ty}}{\tau_u^2} \tag{30}$$

Here, f_{tx}, f_{ty} and τ_u are, respectively, the uniaxial tensile strengths in the x, y directions and the pure shear strength. Note that the material axes are now fixed with respect to a specific frame of reference and it shall be assumed that all stresses and strains for the elastoplastic algorithm are given in the material reference axes. Eq. (29) can be recast in a matrix form as

$$f_1 = (\tfrac{1}{2}\xi^T \mathbf{P}_t \xi)^{\frac{1}{2}} + \tfrac{1}{2}\pi^T \xi \tag{31}$$

where the projection matrix $\mathbf{P}_t$ reads

$$\mathbf{P}_t = \begin{bmatrix} \frac{1}{2} & -\frac{1}{2} & 0 \\ -\frac{1}{2} & \frac{1}{2} & 0 \\ 0 & 0 & 2\alpha \end{bmatrix} \tag{32}$$

the projection vector π reads

$$\pi = \{1 \;\; 1 \;\; 0\}^T \tag{33}$$

the reduced stress vector ξ reads

$$\xi = \sigma - \eta \tag{34}$$

the stress vector σ and the back stress vector η read

$$\begin{aligned} \sigma &= \{\sigma_x \;\; \sigma_y \;\; \tau_{xy}\}^T \\ \eta &= \{\bar{\sigma}_{t1}(\kappa_t) \;\; \bar{\sigma}_{t2}(\kappa_t) \;\; 0\}^T \end{aligned} \tag{35}$$

Exponential tensile softening is considered for both equivalent stress-equivalent strain diagrams, with different fracture energies (G_{fx} and G_{fy}) for each yield value, which reads

$$\bar{\sigma}_{t1} = f_{tx}\exp\left(-\frac{h f_{tx}}{G_{fx}}\kappa_t\right) \qquad \bar{\sigma}_{t2} = f_{ty}\exp\left(-\frac{h f_{ty}}{G_{fy}}\kappa_t\right) \tag{36}$$

It is noted that the equivalent length h, cf. eq. (25), can lead to a snap-back at the constitutive model if the element size is large. Then, the concept of fracture energy which has been assumed is no longer satisfied. In such a case, the strength limit has to be reduced in order to obtain an objective fracture energy by a sudden stress drop, resulting at a certain stage in brittle failure, see Rots (1988). A non-associated plastic potential g_1

$$g_1 = (\tfrac{1}{2}\xi^T \mathbf{P}_g \xi)^{\frac{1}{2}} + \tfrac{1}{2}\pi^T \xi \tag{37}$$

is considered, where the projection matrix $\mathbf{P}_g$ represents the Rankine plastic flow and reads

$$\mathbf{P}_g = \begin{bmatrix} \frac{1}{2} & -\frac{1}{2} & 0 \\ -\frac{1}{2} & \frac{1}{2} & 0 \\ 0 & 0 & 2 \end{bmatrix} \tag{38}$$

The inelastic behavior is described by a strain softening hypothesis, cf. eq. (7), given by the maximum principal plastic strain $\dot{\varepsilon}_1^p$ as

$$\dot{\kappa}_t = \dot{\varepsilon}_1^p = \frac{\dot{\varepsilon}_x^p + \dot{\varepsilon}_y^p}{2} + \tfrac{1}{2}\sqrt{(\dot{\varepsilon}_x^p - \dot{\varepsilon}_y^p)^2 + (\dot{\gamma}_{xy}^p)^2} \tag{39}$$

which reduces to the particularly simple expression[1]

$$\dot{\kappa}_t = \dot{\lambda}_t \tag{40}$$

5.1.3 A Hill type criterion

The simplest yield surface that features different compressive strengths along the material axes is a rotated centered ellipsoid in the full plane stress space (σ_x, σ_y and τ_{xy}). The expression for such a quadric is

$$f_2 = A\sigma_x^2 + B\sigma_x\sigma_y + C\sigma_y^2 + D\tau_{xy}^2 - 1 = 0 \tag{41}$$

where A, B, C and D are four material parameters such that $B^2 - 4AC < 0$, in order to ensure convexity. For the numerical implementation the yield surface can be advantageously recast in a square root matrix form and the variables can be defined in a more amenable way. Thus, the proposed yield surface is rewritten as

$$f_2 = (\tfrac{1}{2}\sigma^T \mathbf{P}_c \sigma)^{\frac{1}{2}} - \bar{\sigma}_c(\kappa_c) \tag{42}$$

where the projection matrix $\mathbf{P}_c$ has been selected as

$$\mathbf{P}_c = \begin{bmatrix} 2\dfrac{\bar{\sigma}_{c2}(\kappa_c)}{\bar{\sigma}_{c1}(\kappa_c)} & \beta & 0 \\ \beta & 2\dfrac{\bar{\sigma}_{c1}(\kappa_c)}{\bar{\sigma}_{c2}(\kappa_c)} & 0 \\ 0 & 0 & 2\gamma \end{bmatrix} \tag{43}$$

the yield value $\bar{\sigma}_c$ is given by

$$\bar{\sigma}_c = \sqrt{\bar{\sigma}_{c1}\bar{\sigma}_{c2}} \tag{44}$$

and the scalar κ_c controls the amount of hardening and softening. The current yield stress values along the materials axes ($\bar{\sigma}_{c1}(\kappa_c)$ and $\bar{\sigma}_{c2}(\kappa_c)$) follow the inelastic law given below as a function of the material compressive strengths along the material axes, respectively f_{mx} and f_{my}. It is noted that the β and γ values introduced in eq. (43) are additional material parameters that determine the shape of the yield surface. The parameter β controls the coupling between the normal stress values, i.e. rotates the yield surface around the shear stress axis, and the parameter γ controls the shear stress contribution to failure.

The inelastic law proposed in the previous section for the elliptical cap is again adopted here. Parabolic hardening followed by parabolic/exponential softening is considered for both equivalent stress-equivalent strain diagrams, with different compressive fracture energies (G_{fcx} and G_{fcy}) along the material axes. The problem of mesh objectivity of the analyses with strain softening materials is a well debated issue, at least for tensile behavior, and the stress-strain diagram must be adjusted

according to a characteristic length h to provide an objective energy dissipation. The inelastic law shown in Fig. 12 features hardening, softening and a residual plateau of ideally plastic behavior. A redefined compressive fracture energy G_{fci} (shaded area in Fig. 12) corresponds only to the local contribution of the $\bar{\sigma}_{\mathrm{ci}} - \kappa_{\mathrm{c}}$ diagram, where the subscript i refers to the material axis. The peak strength value is assumed to be reached simultaneously on both materials axes, i.e. isotropic hardening, followed by anisotropic softening as determined by the different fracture energies. For practical reasons, it is assumed that all the stress values for the inelastic law are determined from the peak value $\bar{\sigma}_{\mathrm{pi}} = f_{\mathrm{mi}}$ as follows: $\bar{\sigma}_{\mathrm{ii}} = \frac{1}{3} f_{\mathrm{mi}}$, $\bar{\sigma}_{\mathrm{mi}} = \frac{1}{2} f_{\mathrm{mi}}$ and $\bar{\sigma}_{\mathrm{ri}} = \frac{1}{10} f_{\mathrm{mi}}$. The equivalent plastic strain κ_{p}, corresponding to the peak compressive strength, is assumed to be an additional material parameter.

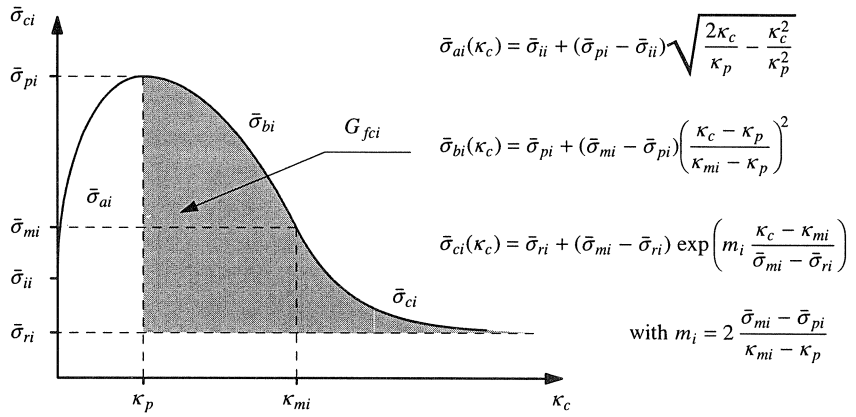

Fig. 12. Hardening/softening law for compression.

An associated flow rule and a work hardening/softening hypothesis are considered. This yields, upon substitution in eq. (10),

$$\dot{\kappa}_{\mathrm{c}} = \frac{1}{\bar{\sigma}_{\mathrm{c}}} \sigma^{\mathrm{T}} \dot{\varepsilon}^{\mathrm{p}} = \dot{\lambda}_{\mathrm{c}} \tag{45}$$

5.2 *Comparison with experimental data of masonry strength*

The most complete strength data of biaxially loaded masonry is given by Page (1981,1983) who tested 102 panels of half-scale solid clay brick masonry, with dimensions $360 \times 360 \times 50\ mm^3$. The panels were loaded proportionally in the principal stress directions σ_1 and σ_2 along different orientations θ with respect to the material axes. The comparison between the experimental values and the model is given in Fig. 13. Globally, good agreement is found. The uniaxial compressive strength parallel to the bed joints seems to be overpredicted by the model, see Fig. 13a, which is due to a debatable definition of failure in the experiments for these loading conditions (early splitting of the bed joints in tension).

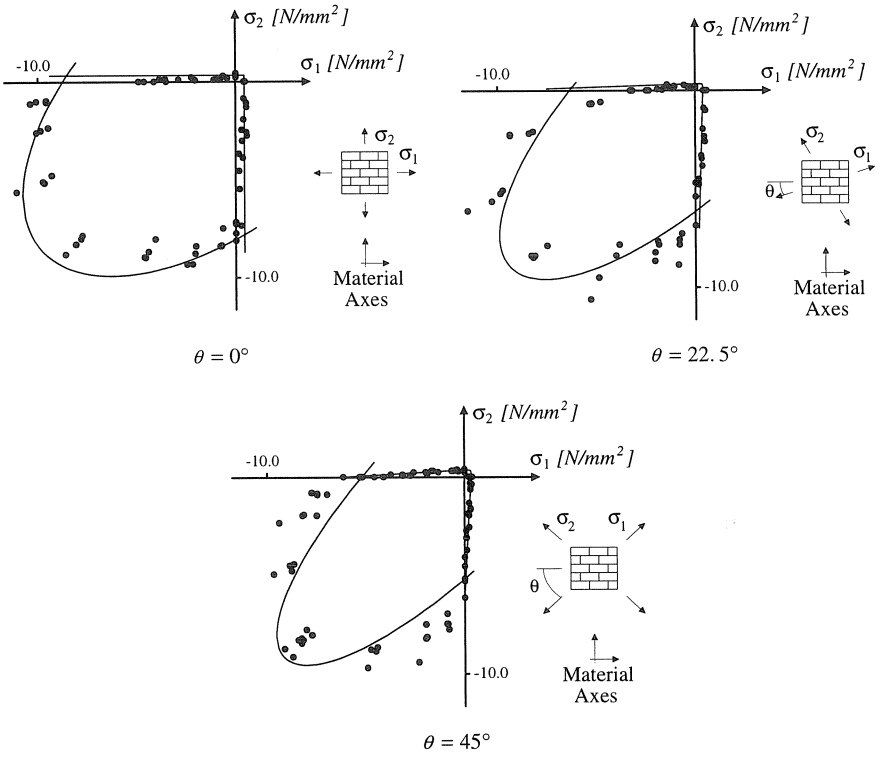

Fig. 13. Comparison between the plasticity model and experimental results from Page (1981,1983). Material parameters: $f_{tx} = 0.43\ N/mm^2$; $f_{ty} = 0.32\ N/mm^2$; $f_{mx} = 8.74\ N/mm^2$; $f_{my} = 8.03\ N/mm^2$; $\alpha = 1.26$; $\beta = -1.17$; $\gamma = 9.59$.

5.3 *Example of application*

It has been pointed out before in this article that, traditionally, experiments in shear walls have been adopted by the masonry community as the most common in-plane large test. In this study, attention is devoted to the results of hollow clay brick masonry shear wall, denoted by wall W, obtained at ETH Zurich, see Ganz and Thürlimann (1984). This test is well suited for the validation of the model, not only because they are large and feature well distributed cracking, but also because most of the parameters necessary to characterize the model are available from biaxial tests. Fig. 14 shows the geometry of the wall, which consists of a masonry panel of $3600 \times 2000 \times 150\ mm^3$ and two flanges of $150 \times 2000 \times 600\ mm^3$. Additional boundary conditions are given by two concrete slabs placed in the top and bottom of the specimen. Initially, the wall is subjected to a vertical load uniformly distributed over the length of the wall, which equals $0.61\ N/mm^2$. This is followed by the application of a horizontal force F on the top slab along a horizontal displacement d.

The experimental crack patterns at peak and ultimate load are shown in Fig. 15. The wall shows a very ductile response with tensile and shear failure along the diagonal stepped cracks.

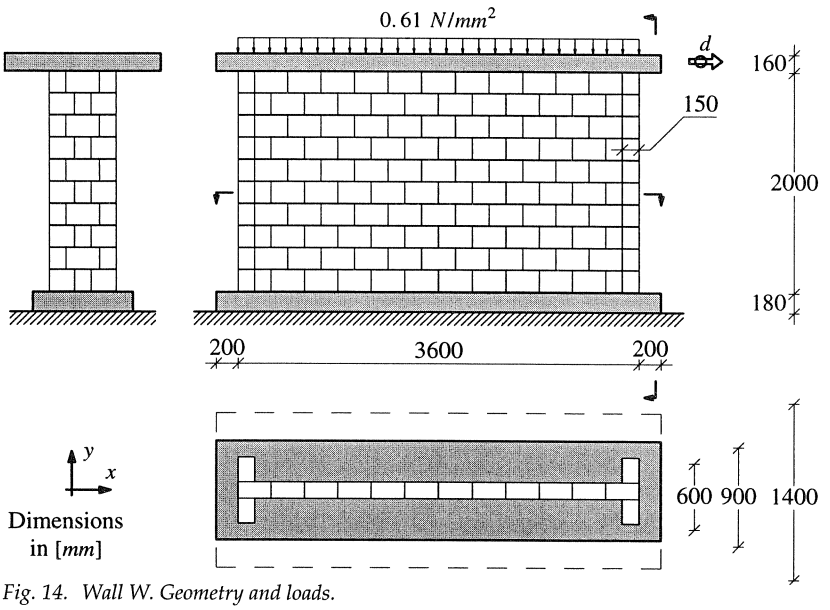

Fig. 14. Wall W. Geometry and loads.

For the numerical analysis linear plane stress continuum elements and constant strain triangles in a cross diagonal patch with full Gauss integration were utilized. A regular mesh of 24 × 15 4-noded quadrilaterals is used for the panel and 2 × 15 cross diagonal patches of 3-noded triangles were used for each flange. The analysis was carried out with indirect displacement control with line searches, whereas the snap-backs are traced with COD control over the most active crack. It is noted that the self-weight of the wall and the top slab is also considered in the analyses. The properties of the composite material are obtained from Ganz and Thürlimann (1982), see Table 4 and Table 5. It is noted that the flanges have the width of a single unit and the failure in the x direction (equivalent to the out-of-plane direction of the panel) is determined by the tensile and compressive strength of the clay brick. These new inelastic properties of the flanges read: $f_{tx} = 0.68\ N/mm^2$ and $f_{mx} = 9.5\ N/mm^2$.

Table 4. Wall W. Elastic properties.

E_x	E_y	v_{xy}	G_{xy}
2460 N/mm^2	5460 N/mm^2	0.18	1130 N/mm^2

The comparison between numerical and experimental load-displacement diagrams is given in Fig. 16. Good agreement is found. The low initial vertical load combined with the confinement provided by the flanges and the top concrete slab yields an extremely ductile behavior.
The unloading found at $d \approx 2.0\ mm$ is due to the mode I crack opening of the left flange.

Table 5. Wall W. Inelastic properties.

Tension regime					
f_{tx}	f_{ty}	α	G_{fx}	G_{fy}	
0.28 N/mm^2	0.05 N/mm^2	1.73	0.02 Nmm/mm^2	0.02 Nmm/mm^2	
Compression regime					
f_{mx}	f_{my}	β	γ	G_{fcx}	G_{fcy}	κ_p
1.87 N/mm^2	7.61 N/mm^2	–1.05	1.20	5.0 Nmm/mm^2	10.0 Nmm/mm^2	8×10^{-4}

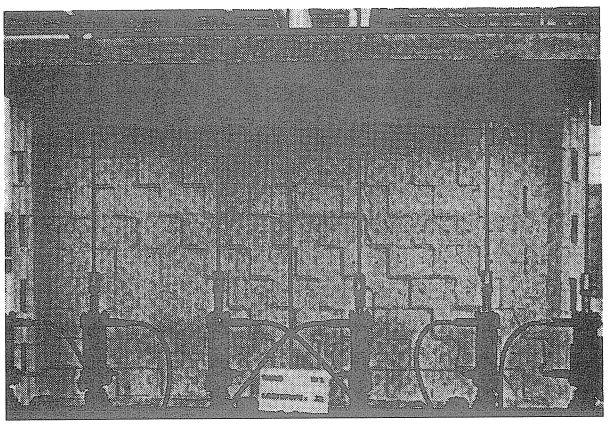

(a)

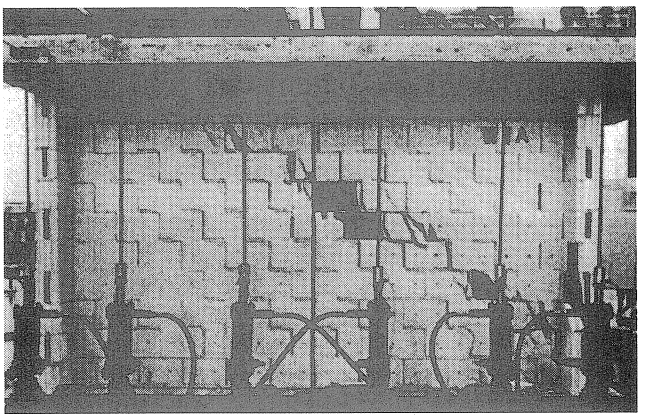

(b)

Fig. 15. Wall W. Experimental failure patterns: (a) peak; (b) end stage, Ganz and Thürlimann (1984).

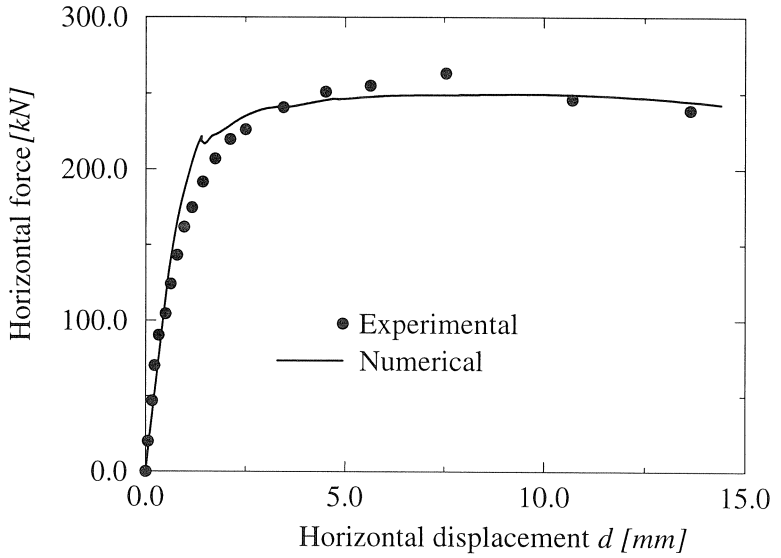

Fig. 16. Wall W. Load - displacement diagrams.

The behavior of the wall is depicted in Fig. 17 and Fig. 18 in terms of deformed meshes, where the center node of the crossed diagonal patch of the flanges is not shown in order to obtain a more legible picture, and cracked Gauss points. Cracks are plotted normal to the tensile principal plastic strain directions with a thickness proportional to the tensile equivalent plastic strain, being the lowest 5% values discarded in order to obtain legible pictures. The comparison between experimental and numerical results is more difficult than in the case of micro-models because units and joints are not modeled. However, reasonable agreement seems to be found. Initially, extensive diagonal cracking of the panel is found, see Fig. 17b. This is accompanied by flexural cracking of the left flange. At this stage, cracking of the panel is, basically, governed by the Mohr's circle as a relatively uniform state of stress in the panel is found. Upon increasing horizontal loading, cracking tends to concentrate in a large shear band going from one corner of the specimen to the other, which is accompanied by flexural cracking of the right flange, see Fig. 18. At this ultimate stage, a well defined failure mechanism is formed with a final shear band going from one corner of the specimen to the other and intersecting the flanges. This means that cracks rotate significantly after initiation governed by Mohr's circle to failure in a sort of shear band, which agrees well with the experiments, see Fig. 15. Even at the ultimate stage the stress values are considerably below the maximum compressive strength in the vertical direction which confirms that failure is exclusively governed by the tension regime.

It is not surprising that the plasticity model can capture the significantly large rotations of cracks because the Rankine yield surface resembles the rotating crack model, see Feenstra (1993) and Lourenço *et al.* (1995).

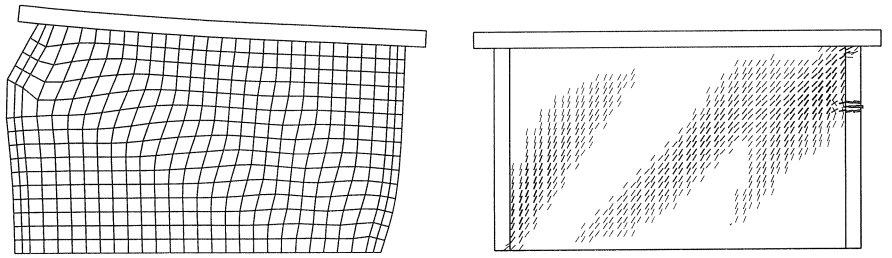

(a) (b)

Fig. 17. Wall W. Results of the analysis at a displacement of 2.0 mm: (a) (incremental) deformed mesh; (b) cracks

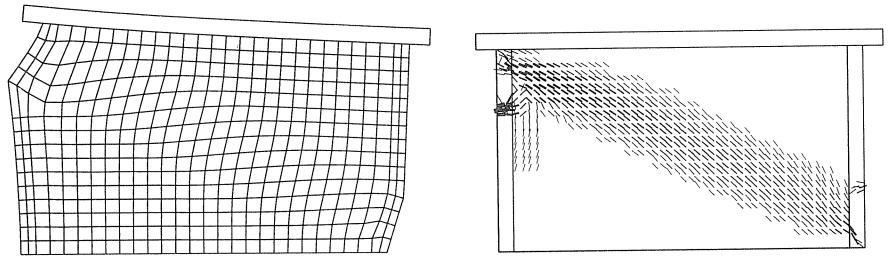

(a) (b)

Fig. 18. Wall W. Results of the analysis at a displacement of 12.0 mm: (a) deformed mesh; (b) cracks.

6 Final remarks

Masonry is a composite material that consists of units and mortar, normally arranged in a periodic manner. The interface between units and mortar acts as a plane of weakness and is, largely, responsible for the inelastic behavior. A detailed modeling strategy must then include units, mortar and interface. However, such a modeling strategy is unwieldy and the computational inefficiency becomes prohibitive in the analysis of large structures. Simplified approaches are thus preferred in the present article, namely, a *micro-modeling* strategy, where joints are modeled with zero-thickness interface elements, and a *macro-modeling* strategy, where a relation is established between average masonry stresses and average masonry strains, under the assumption of a homogeneous material.
In a micro-modeling approach, units are modeled with continuum elements and joints are modeled with interface elements. All inelastic phenomena are lumped in the relatively weak joints via a composite interface model. This (plasticity) model comprehends three different failure mechanisms, namely, a straight tension cut-off for mode I failure, the Coulomb friction model for mode II failure as well as an elliptical cap for compression and combined shear/compression failure.
Validation of the model against an experiment carried out in a shear wall was successful. This gives a good impression about the adopted modeling strategy and provides a good understanding of the failure mechanisms involved in the analyzed structures. The (micro-)model is particularly suited for small structures and structural details where the interaction between units and mortar is of pri-

mary interest. It is noted that, for large structures, the memory and time requirements become too large and, if a compromise between accuracy and economy is needed, a macro-modeling strategy is likely to be more efficient.

In a macro-modeling approach, units and joints are smeared out in a homogeneous continuum where a relation is established between average masonry stresses and average masonry strains. An orthotropic continuum model has been presented, which consists of a Rankine type yield criterion for tensile failure and a Hill type yield criterion for compressive failure. It is assumed that the failure mechanism of masonry loaded in tension and compression is governed by crack growth at the micro-level. Furthermore it is assumed that the internal damage associated with each failure mechanism can be modeled using internal parameters which are related to a fracture energy in tension and a compressive fracture energy. This energy-based (plasticity) model resorts to the well known crack band theory to obtain objective results with respect to the finite element mesh size. The model is capable of predicting independent, in the sense of completely diverse, behavior along the material axes. A comparison with experimental observations in a shear wall test shows good agreement.

7 Acknowledgements

This research has been supported financially by the Netherlands Technology Foundation (STW) under grant DCT 33.3052.

8 References

ANTHOINE, A. (1992), *In-plane behaviour of masonry: A literature review*. Report EUR 13840 EN, Comission of the European Communities, JRC - Institute for Safety Technology, Ispra, Italy.

BAŽANT, Z.P. and OH, B.H. (1983), Crack band theory for fracture of concrete. *Materials and Structures*, RILEM, **93(16)**, p. 155–177.

BESSELING, J.F. (1958), A theory of elastic, plastic and creep deformations of an initially isotropic material showing anisotropic strain-hardening, creep recovery and secondary creep. *J. Appl. Mech.*, **22**, p. 529–536.

BORST, R. DE and FEENSTRA, P.H. (1990), Studies in anisotropic plasticity with reference to the Hill criterion. *Int. J. Numer. Methods Engrg.*, **29**, p. 315–336.

CUR (1994), *Structural masonry: a experimental/numerical basis for practical design rules* (in Dutch). Report 171, CUR, Gouda, The Netherlands.

DETHIER, J. (1982), *Down to Earth: Mud architecture, an old idea, a new future*. Thames and Hudson, London, UK.

DRUCKER, D.C., GIBSON, R.E. and HENKEL, D.J. (1957), Soil mechanics and work hardening theories of plasticity. *Trans. ASCE*, **122**, p. 338–346.

FEENSTRA, P.H. (1993), *Computational aspects of biaxial stress in plain and reinforced concrete*. Dissertation, Delft University of Technology, Delft, The Netherlands.

FEENSTRA, P.H. and BORST, R. DE (1996), A composite plasticity model for concrete. *Int. J. Solids Structures*, **33(5)**, p. 707–730.

GANZ, H.R. and THÜRLIMANN, B. (1982). *Tests on the biaxial strength of masonry* (in German). Report No. 7502-3, Institute of Structural Engineering, ETH Zurich, Zurich, Switzerland.

GANZ, H.R. and THÜRLIMANN, B. (1984), *Tests on masonry walls under normal and shear loading* (in German). Report No. 7502-4, Institute of Structural Engineering, ETH Zurich, Zurich, Switzerland.

HILL, R. (1948), A theory of the yielding and plastic flow of anisotropic metals. *Proc. Roy. Soc.*, (London) A, **193**, p. 281–288.

HOFSTETTER, G., SIMO, J.C. and TAYLOR, R.L. (1993), A modified cap model: closest point solution algorithms. *Comp. Struct.*, **46(2)**, p. 203-214.

KOITER, W.T. (1953), Stress-strain relations, uniqueness and variational theorems for elastic-plastic materials with a singular yield surface. *Q. Appl. Math.*, **11(3)**, p. 350–354.

LOURENÇO, P.B. (1996), *Computational strategies for masonry structures*. Dissertation, Delft University of Technology, Delft, The Netherlands.

LOURENÇO, P.B., ROTS, J.G. and FEENSTRA, P.H. (1995), A 'tensile' Rankine type orthotropic model for masonry, in: *Computer methods in structural masonry 3*, eds. G.N. Pande and J. Middleton, Books & Journals International, Swansea, UK.

PAGE, A.W. (1981), The biaxial compressive strength of brick masonry. *Proc. Intsn. Civ. Engrs.*, Part 2, **71**, p. 893–906.

PAGE, A.W. (1983), The strength of brick masonry under biaxial compression-tension. *Int. J. Masonry Constr.*, **3(1)**, p. 26–31.

PLUIJM, R. VAN DER (1993), Shear behaviour of bed joints, in: *Proc. 6th North American Masonry Conf.*, eds. A.A. Hamid and H.G. Harris, Drexel University, Philadelphia, Pennsylvania, USA, p. 125–136.

RAIJMAKERS, T.M.J. and VERMELTFOORT, A.Th. (1992), *Deformation controlled tests in masonry shear walls* (in Dutch). Report B-92-1156, TNO-BOUW, Delft, The Netherlands.

ROSCOE, K.H. and BURLAND, J.B. (1968), On the generalized stress-strain behaviour of "wet" clay, in: *Engineering Plasticity*, eds. J. Heyman and F.A. Lekie, Cambridge University Press, London, UK, p. 535-609.

ROTS, J.G. (1988), *Computational modeling of concrete fracture*. Dissertation, Delft University of Technology, Delft, The Netherlands.

SIMO, J.C., KENNEDY, J.G. and GOVINDJEE, S. (1988), Non-smooth multisurface plasticity and visco-plasticity. Loading/unloading conditions and numerical algorithms. *Int. J. Numer. Methods Engrg.*, **26**, p. 2161–2185.

SWAN, C.C. and CAKMAK, A.S. (1994), A hardening orthotropic plasticity model for non-frictional composites: Rate formulation and integration algorithm. *Int. J. Numer. Methods Engrg.*, **37**, p. 839–860.

TSAI, S.W. and WU, E.M. (1971), A general theory of strength of anisotropic materials, *J. Composite Mat.*, **5**, p. 58–80.